Landau Theory Description of Autferroicity

Jun-Jie Zhang,[1,2] Boris I. Yakobson,[2,*] and Shuai Dong[1,†]
[1]Key Laboratory of Quantum Materials and Devices of Ministry of Education, School of Physics, Southeast University, Nanjing 211189, China
[2]Department of Materials Science and NanoEngineering, Rice University, Houston, Texas 77005, USA

(Received 11 September 2024; revised 19 January 2025; accepted 2 May 2025; published 28 May 2025)

Autferroics, recently proposed as a sister branch of multiferroics, exhibit strong intrinsic magnetoelectricity, but ferroelectricity and magnetism are mutually exclusive rather than coexisting. Here, a general model is considered based on the Landau theory, to clarify the distinction between multiferroics and autferroics by qualitative change-rotation in a Landau free energy landscape and in particular phase mapping. The $TiGeSe_3$ exemplifies a factual material, whose first-principles computed Landau coefficients predict its autferroicity. Our investigation paves the way for an alternative avenue in the pursuit of intrinsically strong magnetoelectrics.

DOI: 10.1103/PhysRevLett.134.216801

Introduction—The interplay of magnetism and ferroelectricity is one of the core physical issues of condensed matter, providing plenty of functionalities for applications. In the past two decades, multiferroics, with coexisting polar and magnetic orders in single phases [1–3], have been extensively studied for their prominent magnetoelectric (ME) coupling, which allows for the control of electric dipoles through magnetic fields or the manipulation of spins through electric fields. The magnetoelectric spin-orbit devices based on these ME functions bring promising perspectives for for high-speed, low-power information processing [4].

However, to some degree, magnetism and polarity intrinsically suppress each other, preventing ideal magnetoelectricity in multiferroics, thus it always results in a trade-off between magnetism and polarity, as well as their coupling. For example, in type-I multiferroics (e.g., $BiFeO_3$) [5], ME couplings are weak despite strong ferroelectricity, while in type-II multiferroics (e.g., $TbMnO_3$) [6], polarizations are faint but fully switchable by magnetic fields. Such a trade-off seems unavoidable and almost impossible to be perfectly resolved in the framework of multiferroics.

Very recently, a new kind of hybrid ferroicity was proposed as a sister branch of multiferroics, dubbed *alterferroicity* [7]. To stay clear of the newly emerged field of *altermagnetism*, the term we use henceforth is *autferroicity*, prefix *aut* being Latin for "or, either." In autferroics, ferroelectricity and magnetism are mutually exclusive rather than coexisting, yet they can be controlled by external fields. The first candidate material is a transition-metal trichalcogenide $TiGe_{1-x}Sn_xTe_3$ [7]. In this two-dimensional monolayer, ferroelectric and antiferromagnetic states can be (meta)stable and compete with each other, leading to the so-called seesaw-type magnetoelectricity [7]. In fact, similar ferroelectric-antiferromagnetic competitions and transitions have also been theoretically predicted in $CrPS_3$ [8] and experimentally reported in $[1-x](Ca_{0.6}Sr_{0.4})_{1.15}Tb_{1.85}Fe_2O_7 - [x]Ca_3Ti_2O_7$ series [9], although the concept of autferroicity had not been introduced at that time. As an emerging topic, autferroicity is much less known than multiferroicity.

In this Letter, a general and minimal model for autferroicity is considered based on the Landau theory. By taking the exclusion term in the Landau free energy expression, this model can describe the magnetoelectricity of autferroics elegantly. Then, by employing density functional theory (DFT) calculations, $TiGeSe_3$ and $TiSnSe_3$ monolayer are selected as the benchmark of our theory, where the ME coupling strengths are quantitatively calculated. According to the Landau theory, the $TiGeSe_3$ monolayer potentially exhibits antiferroicity, whereas $TiSnSe_3$ does not.

Model—According to the Landau theory, the canonical expression of temperature (T) dependent magnetoelectric Landau free energy (F) can be written as [10,11]

$$F(P,M,T) = \left[-a\left(1-\frac{T}{T_P}\right)P^2 + bP^4\right] + \left[-d\left(1-\frac{T}{T_M}\right)M^2 + eM^4\right] + cP^2M^2, \quad (1)$$

where P and M are order parameters (OPs) for ferroelectricity and ferromagnetism, respectively. T_P and T_M are the transition temperatures for independent ferroelectricity and ferromagnetism, respectively. In fact, the first (second) two terms are canonical Landau-type free energy of ferroelectricity (ferromagnetism). All the coefficients are

*Contact author: biy@rice.edu
†Contact author: sdong@seu.edu.cn

positive, leading to the double-well energy curves as a function of P or M below their transition temperatures. For antiferromagnetism, it is straightforward to formally replace M with the antiferromagnetic order parameter L. Thus, in the following, only the symbol M is used without loss of generality. The last term is the magnetoelectric coupling energy, where c is the coupling strength. Note that such a biquadratic term generally works for ferroelectromagnets of all symmetries, while other lower order coupling terms may exist but are specialized for some specific systems like type-II multiferroics or hybrid improper ferroelectrics [see End Matter (EM) for details] [1,12–18].

Zero-T results—Obviously, if $c = 0$, the ferroelectricity and magnetism are entirely decoupled. Then the lowest Landau free energy can be obtained from $\partial F/\partial M = 0$ and $\partial F/\partial P = 0$, leading to nonzero equilibrium $P_s = \sqrt{(a/2b)}$ and $M_s = \sqrt{(d/2e)}$ at $T = 0$. With a small negative c, Eq. 1 was frequently used to describe conventional multiferroic systems successfully [19–22].

Here we focus on positive c, corresponding to the exclusion between polarity and magnetism, which can describe the autferroicity (and widely exists in multiferroicity). First, the ground state at $T = 0$ is discussed. With a positive c, the equilibrium M_e or P_e can be obtained straightforwardly as follows:

$$M_e = \sqrt{\frac{d - cP^2}{2e}} \quad \text{or} \quad P_e = \sqrt{\frac{a - cM^2}{2b}}. \tag{2}$$

By substituting Eq. 2 into Eq. 1, the Landau free energy becomes

$$F(P, M_e) = -\frac{d^2}{4e} + \left(-a + \frac{dc}{2e}\right)P^2 + \left(b - \frac{c^2}{4e}\right)P^4,$$
$$F(P_e, M) = -\frac{a^2}{4b} + \left(-d + \frac{ac}{2b}\right)M^2 + \left(e - \frac{c^2}{4b}\right)M^4, \tag{3}$$

where the depolarized and demagnetized effects from the ME term are clear.

Let us analyze the magnetoelectric behavior with gradually increasing c from 0. For case 1, when $c < 2bd/a \equiv c_m$ and $c < 2ae/d \equiv c_p$, the system works as a multiferroic, with spontaneous polarization $P_s = \sqrt{[d(c_p - c)]/(c_m c_p - c^2)}$ and magnetization $M_s = \sqrt{[a(c_m - c)]/(c_m c_p - c^2)}$, i.e., a type-I multiferroic solution with independent origins of P and M [23].

In all of following cases, we assume $c_m > c_p$ if not noted explicitly, while the opposite condition $c_m < c_p$ will lead to symmetric results by interchanging the OPs M and P. Furthermore, both P_s and M_s have been normalized to 1. For case 2, if $c_p < c < \sqrt{c_m c_p}$, the condition for spontaneous nonzero polarization cannot be satisfied, and then the solution can only be $[P_s = 0,\ M_s = \sqrt{[a(c_m - c)]/(c_m c_p - c^2)}]$. For case 3, if $\sqrt{c_m c_p} < c < c_m$, the coefficients of P^4 and M^4 in Eqs. 3 become negative, which lead to diverging P_s and M_s. In this case, Eqs. 3 are invalid. The solution for Eq. 1 remains the same as for case 2. Thus, cases 2 and 3 can be unified as $c_p < c < c_m$, leading to a pure magnetic phase. For case 4, if $c > c_m$, the solution for Eq. 1 becomes $[P_s = 0,\ M_s = \sqrt{[a(c_m - c)]/(c_m c_p - c^2)}]$ or $[M_s = 0,\ P_s = \sqrt{[d(c_p - c)]/(c_m c_p - c^2)}]$, i.e., an autferroic solution.

A similar analysis can be done for negative c. For case 5, if $-c < \sqrt{c_m c_p}$, the result is similar to the aforementioned case 1, i.e., a multiferroic solution. For case 6, $-c > \sqrt{c_m c_p}$, Eq. 1 becomes inadequate to describe ferroics, while higher order P^6 and M^6 terms are mandatory to avoid diverging P_s and M_s. The ground state phase diagram and corresponding evolution of OPs are summarized in Fig. 1(a). In this sense, the autferroicity naturally owns stronger ME coupling than the type-I multiferroics, characterized by coefficient c.

Typical energy landscapes $F(P, M)$ with various c are distinct. When c has a small value (regardless of being negative or positive), the energy landscape shows isodepth

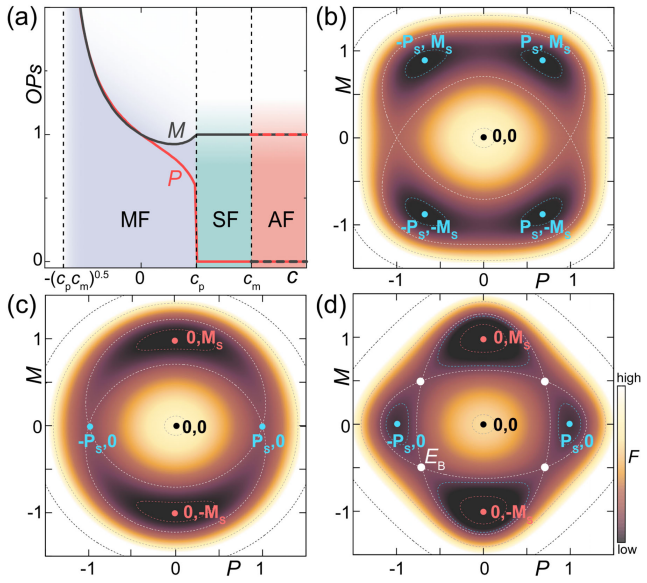

FIG. 1. Ground state solution of Eq. 1. (a) Phase diagram as a function of ME coefficient c. MF: (type I) multiferroic phase; SF: single-ferroic phase (i.e., magnetic if $c_m > c_p$); AF: autferroic phase. The order parameters (OPs) are shown as curves. In the autferroic region, the dashed lines denote the alternative solutions, $(P_s, 0)$ or $(0, M_s)$, which cannot exist simultaneously. If $c_m < c_p$, the curves of M and P are interchanged, and the SF region is ferroelectric. (b)–(d) Typical energy landscapes $F(P, M)$ for (b) MF, (c) SF, and (d) AF. E_B in (d) indicates the energy barrier from $(\pm P_s, 0)$ to $(0, \pm M_s)$.

quadruple wells at $(\pm P_s, \pm M_s)$ [Fig. 1(b)], as in the type-I multiferroics with coexisting ferroic orders. In the middle positive c region, one ferroic order (i.e., P if $c_m > c_p$ or M if $c_m < c_p$) is completely suppressed, leading to double energy wells [Fig. 1(c)]. When the positive c is large enough, the energy landscape of autferroic phase restores quadruple wells in Fig. 1(d), but at positions $(\pm P_s, 0)$ and $(0, \pm M_s)$ rotated by $\pi/4$ relative to Fig. 1(b).

Another fact for autferroic is that its quadruple wells are double-degenerated in energy. If $c_m > c_p$ $(c_m < c_p)$, the magnetic (ferroelectric) state is more favored. There is an energy barrier (E_B) between neighboring $(\pm P_s, 0)$ and $(0, \pm M_s)$ wells [Fig. 1(d)], making the ferroelectric (magnetic) phase a metastable one. This energy barrier is determined by ME coupling strength, as derived in Supplemental Material (SM) [24].

Finite-T results—At finite temperatures, the coefficients c_m and c_p become

$$C_M(T) = c_m\gamma(T), \qquad C_P(T) = c_p/\gamma(T), \tag{4}$$

where $\gamma(T) = [T_P(T_M - T)/T_M(T_P - T)]$ is the temperature-dependent dimensionless factor $[\gamma(0) = 1]$.

When $T < T_P < T_M$ [Fig. 2(a)], the finite temperature leads to $\gamma(T) > 1$. Here, three aforementioned ground states are analyzed. (1) For the autferroic ground state, i.e., $c > c_m > c_p$, it is natural to expect a critical temperature T_P^* between 0 and T_P to satisfy the condition $C_P(T_P^*) < c = C_M(T_P^*)$. When $T_P^* < T < T_M$, the system is no longer autferroic, but becomes single-ferroic with only magnetic order active. (2) For the single-ferroic (i.e., magnetic) ground state, i.e., $c_p < c < c_m$, the system does not have a transition point when $T < T_P$. (3) For the multiferroic ground state, i.e., $c < c_p < c_m$, there must be a T_M^* to satisfy $C_P(T_M^*) = c < C_M(T_M^*)$. Thus the system becomes magnetic only when $T > T_M^*$. Finally, all three become nonferroic when $T > T_M$.

The $T < T_M < T_P$ case is more complex [Fig. 2(b)], as $0 < \gamma(T) < 1$. This case exhibits several different behaviors compared to the $T < T_P < T_M$ situation. (1) For the autferroic case, $C_P(T)$ will go beyond c at T_M^*; then the system becomes ferroelectric state $(T_M^* < T < T_P)$. (2) For the single-ferroic case, two intermediate phases are identified: multiferroic or autferroic if c is relatively small or large, respectively, before the emerging of the ferroelectric phase. (3) For the multiferroic ground state, the system will become magnetic only when $T > T_M^*$. Finally, all states become nonferroic when $T > T_P$.

These two phase diagrams are obtained at the mean field level without thermal fluctuations. In real systems, the transition temperatures will be affected by fluctuations, especially for metastable phases. Here, four cases I–IV as indicated in Figs. 2(a)–2(b) are checked using Monte Carlo (MC) methods. Method details can be found in EM4, EM5, and SM [24].

For case I [Fig. 2(c)], MC results indeed confirm that system is type-I multiferroic below T_P^* and becomes a magnetic state between T_P^* and T_M. Despite these qualitative agreements, the T_P^* obtained in our MC simulation is slightly lower than the analytical expectation. This is reasonable since, in the single-ferroic region, there remains local fluctuation of the ferroelectric order (i.e., not exactly zero as in the analytical solution), suppressing local magnetism via the ME coupling.

For case II [Fig. 2(d)], our MC simulations show a sharp transition from the initial (metastable) ferroelectric to

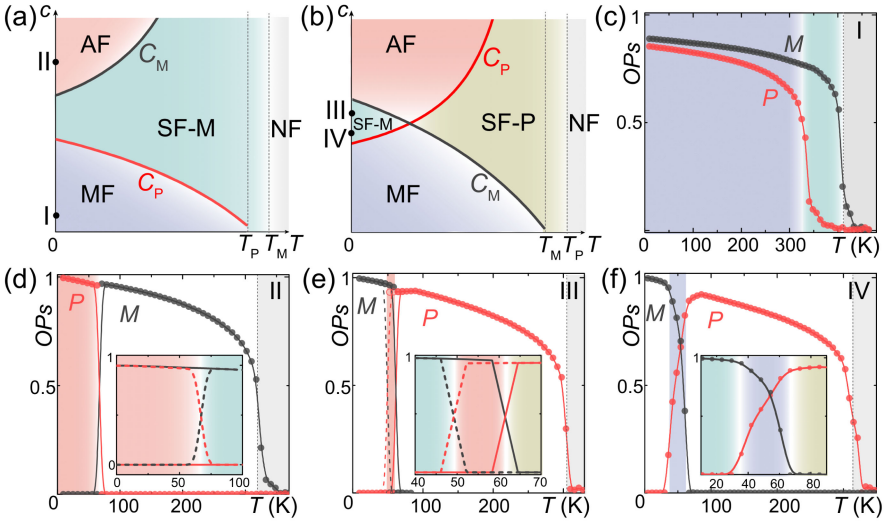

FIG. 2. Solutions of Eq. 1 at finite temperatures. (a)–(b) Analytic phase diagrams in the c-T parameter space. NF: nonferroic state; SF-M (SF-P): single-ferroic magnetic (ferroelectric) phase. Phase boundaries are $C_P(T_P^*)$ (red) and $C_M(T_M^*)$ (black). (a) $T_M > T_P$; (b) $T_P > T_M$. (c)–(f) MC results for four selected cases I–IV, as indicated in (a)–(b). Their corresponding coefficients are listed in Table S1. Insets: enlarged views around the transitions.

magnetic state at T^* much lower than estimated T_P. This T^* is primarily due to the small E_B between the ferroelectric and magnetic phases in autferroics [Fig. 1(d)], which cannot beat the thermal fluctuation. A similar situation is also found in case III [Fig. 2(e)], where the temperature range for the intermediate autferroic region (52–59 K) is much narrower than the analytical 20–88 K, namely, the effective working temperature window for zero-field autferroicity becomes shrunken due to the fact of metastability and thermal fluctuation. Without the metastability (e.g., case IV), the temperature window for the intermediate multiferroic phase is much broader [35–72 K in Fig. 2(f)], slightly narrower than the analytical value (27–84 K).

Material benchmarks—To verify above model results, the $TiGeSe_3$ monolayer is studied as a benchmark, which was predicted to exhibit both magnetic and ferroelectric orders [7]. In $TiGeSe_3$, Ti ions form a honeycomb lattice and each Ti is surrounded by six Se ions, shown in Fig. 3(a), forming a $TiSe_6$ triangular antiprism. Due to the trigonal crystal field, Ti's $3d$ orbitals are split into three groups [Fig. 3(a)]. Our DFT calculations confirm that its magnetic ground state is stripy-type antiferromagnet (S-AFM); see Fig. S2(a) [7,24].

Besides S-AFM, the Ge-Ge pair in the $TiGeSe_3$ monolayer would move along the out-of-plane direction [Fig. 3(a)], driven by the soften polar mode. Taking the nonpolar parent phase as a reference, the DFT energy (E) versus displacement λ [defined in Fig. 3(a)] reveals a typical ferroelectric double-well potential [Fig. 3(b)], where the switching energy barrier E_P is ~200 meV/f.u. [24]. The polarization in the $TiGeSe_3$ monolayer mainly originates from Ge's lone pair electrons [Fig. 3(a)]. Notably, these lone pair electrons, with Se sites acting as bridges, induce a valence change from Ti^{3+} to Ti^{4+}, as identified in the electric structures [Figs. 3(c)–3(d)]. In Fig. 3(c), the d_{z^2} orbital contributes to valence bands in the S-AFM phase ($3d^1$), which is empty ($3d^0$) in the ferroelectric phase [Fig. 3(d)]. Hence, ferroelectric and magnetic phases in $TiGeSe_3$ are mutually exclusive.

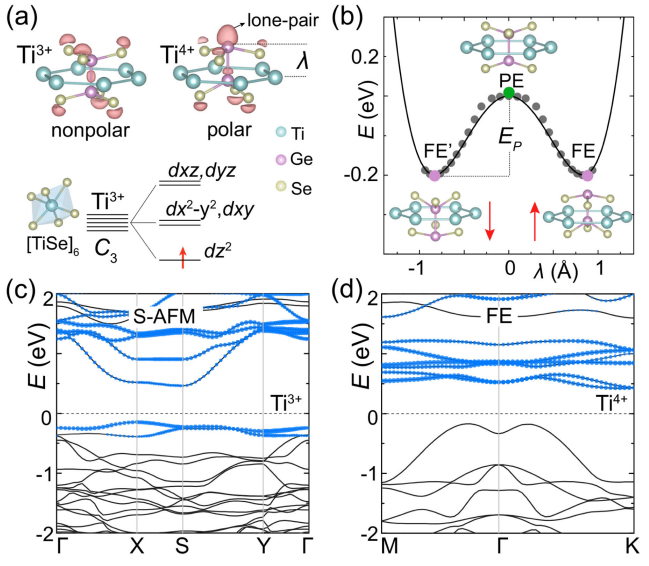

FIG. 3. Benchmark of $TiGeSe_3$ monolayer. (a) Upper: structure of $TiGeSe_3$ monolayer and out-of-plane Ge-Ge pair displacement (λ). Lower: band splitting of Ti's $3d$ orbitals and stripy-type antiferromagnetic (S-AFM) structure. (b) Energy (E) per f.u. as a function of λ. E_P: energy barrier. Dots: DFT-computed energies. Insets: paraelectric and ferroelectric phases with $\pm P$. (c)–(d) Comparison between band structures for (c) S-AFM and (d) ferroelectric (FE) state. Blue: projected Ti's $3d$ orbitals.

Equation 1 can be utilized to further identify the ferroic phases of the $TiGeSe_3$ monolayer at 0 K, specifically distinguishing between the single-ferroic and autoferroic phases. The ferroelectric and magnetic Landau parameters are extracted from DFT energy calculations of selected configurations (λ,M), with a detailed description in EM6. To quantify the ME coefficient of the $TiGeSe_3$ monolayer, a series of small displacements (λ) are artificially introduced into the S-AFM phase, where the spontaneous magnetic moments are fixed [$L = L_s = (M_{s\uparrow} - M_{s\downarrow})/2$, see SM8 [24]] in our DFT calculation. The energy contribution from the magnetoelectric interaction term is $\Delta F(\lambda) = F_{\rm tot} - (-\tilde{a}\lambda^2 + \tilde{b}\lambda^4) - (-dL_s^2 + eL_s^4) = \tilde{c}\lambda^2 L_s^2$, where $\tilde{a} = aZ_\lambda^{*-2}$ and $\tilde{b} = bZ_\lambda^{*-4}$. Here, Z_λ^* is the magnitude of Born effective charge along the displacement λ direction. Hence, the $\Delta F(\lambda)$ as a function of λ follows a parabolic curve [Fig. 5(a)], allowing the ME coefficient $\tilde{c}$ (or $c = \tilde{c}Z_\lambda^{*2}$) to be obtained by fitting the parabolic coefficient $k_c \equiv \tilde{c}L_s^2$.

The fitted $\tilde{c}$ reaches ~890 meV/$(\mu_B$Å$)^2$, satisfying the autferroic requirement of $\tilde{c}_p < \tilde{c}_m < \tilde{c}$ (see Table I). In this scenario, the S-AFM phase serves as the ground state, while the ferroelectric phase is metastable. To verify this state metastability in $TiGeSe_3$, we recalculated the structure with a smaller ferroelectric displacement (e.g., $0.8\lambda_s$, where λ_s is the stable spontaneous atomic displacement) in DFT and initialized with a small magnetic moment. After full lattice relaxation, the system returned to the pure ferroelectric phase, indicating that the pure ferroelectric state is not an energy saddle point. Hence, the $TiGeSe_3$ monolayer exhibits autferroicity, corresponding to case II in Fig. 2(a), which originates from the strong spin-phonon coupling. Based on our MC simulations, the transition from the

TABLE I. Fitted parameters $\tilde{a}$ (meV/Å^2), $\tilde{b}$ (meV/Å^4), d (meV/$\mu_B{}^2$), e (meV/$\mu_B{}^4$), and $\tilde{c}$ [meV/$(\mu_B$Å$)^2$]. Calculated Energy barrier E_B (meV/f.u.) and autferroic transition temperature T_C (K).

	$\tilde{a}$	$\tilde{b}$	d	e	$\tilde{c}_p$	$\tilde{c}_m$	$\tilde{c}$	E_B	T_C
$TiGeSe_3$	390	190	520	260	390	520	890	44	63
$TiSnSe_3$	900	360	60	30	900	40	740	0	0

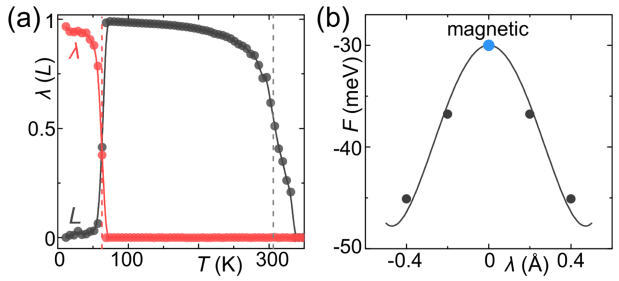

FIG. 4. (a) MC results for autferroic $TiGeSe_3$: displacement λ and magnetic moment L vs. temperature T. The initial ferroelectricity vanishes at ~64 K. (b) DFT evidence for the single-ferroic phase in $TiSnSe_3$. Total Landau free energy F as a function of ferroelectric displacement λ in the Z-AFM phase, with Ti's magnetic moment fixed at $L = L_s$. Blue point, pure magnetic phase at the energy saddle point; dots, DFT-computed energies.

autferroic state to the magnetic state occurs at 63 K for $TiGeSe_3$ [Fig. 4(a)], close to the estimate from Landau equation $T_M^* = 59$ K.

For comparison, we also calculate its sister member $TiSnSe_3$ monolayer. The $TiSnSe_3$ monolayer exhibits behavior similar to that of $TiGeSe_3$; however, in this case, the ferroelectric phase has a lower energy than the ground magnetic state (zigzag-type AFM, Z-AFM). Our fitted results show that $TiSnSe_3$ should not exhibit autferroicity, as it satisfies $\tilde{c}_m < \tilde{c} < \tilde{c}_p$ (Table I), where the ferroelectric phase is stable, and the Z-AFM state corresponds to an energy saddle point. These results can also be further examined through DFT calculations: a series of small ferroelectric displacements λ artificially introduced into the Z-AFM phase of $TiSnSe_3$, with the magnetic moments fixed at $L = L_s$. The resulting total energy F vs λ curve clearly indicates that the pure magnetic state is at an energy saddle point [Fig. 4(b)]. Therefore, the $TiSnSe_3$ monolayer is a single-ferroic material, exhibiting only a stable ferroelectric phase.

In summary, a unified Landau theory model is proposed to describe the mutual exclusion between magnetic and ferroelectric orders in autferroics. In the phase diagram, the autferroic phase appears in the region with stronger magnetoelectric exclusive coupling. Both the ground state and finite temperature effects are demonstrated, with concrete materials as benchmarks. Characteristic of autferroics, the energy barriers separating $\pm M_s$ ($\pm P_s$) are relatively low, promoting rapid thermal fluctuations, which is beneficial to autferroic-based random number generation devices [35,36].

Acknowledgments—Work at SEU (J. Z. and D. S.) was supported by the National Natural Science Foundation of China (Grants No. 12325401, No. 12274069, and No. 12404102), Natural Science Foundation of the Jiangsu Province (Grant No. BK20230806), open research fund of Key Laboratory of Quantum Materials and Devices of the Ministry of Education (Southeast University), and Southeast University Interdisciplinary Research Program for Young Scholars (Grant No. 2024FGC1008). Computer resources at SEU were provided through Big Data Center of Southeast University. Work at Rice (J. Z. and B. I. Y.) was supported by the U.S. Office of Naval Research (No. N00014-22-1-2753). Computer resources at Rice were provided through allocation DMR100029 from the ACCESS program, supported by the National Science Foundation (Grant No. 2138296).

[1] S. Dong, J.-M. Liu, S.-W. Cheong, and Z. Ren, Multiferroic materials and magnetoelectric physics: Symmetry, entanglement, excitation, and topology, Adv. Phys. **64**, 519 (2015).
[2] S. Dong, H. Xiang, and E. Dagotto, Magnetoelectricity in multiferroics: A theoretical perspective, Natl. Sci. Rev. **6**, 629 (2019).
[3] N. A. Spaldin and R. Ramesh, Advances in magnetoelectric multiferroics, Nat. Mater. **18**, 203 (2019).
[4] S. Manipatruni, D. E. Nikonov, C.-C. Lin, T. A. Gosavi, H. Liu, B. Prasad, Y.-L. Huang, E. Bonturim, R. Ramesh, and I. A. Young, Scalable energy-efficient magnetoelectric spin–orbit logic, Nature (London) **565**, 35 (2019).
[5] J. Wang, J. B. Neaton, H. Zheng, V. Nagarajan, S. B. Ogale, B. Liu, D. Viehland, V. Vaithyanathan, D. G. Schlom, U. V. Waghmare, N. A. Spaldin, K. M. Rabe, M. Wuttig, and R. Ramesh, Epitaxial $BiFeO_3$ multiferroic thin film heterostructures, Science **299**, 1719 (2003).
[6] T. Kimura, T. Goto, H. Shintani, K. Ishizaka, T. Arima, and Y. Tokura, Magnetic control of ferroelectric polarization, Nature (London) **426**, 55 (2003).
[7] Z. Wang and S. Dong, Alterferroicity with seesaw-type magnetoelectricity, Proc. Natl. Acad. Sci. U.S.A. **120**, e2305197120 (2023).
[8] W. Gao, J. Zhao, and J. R. Chelikowsky, Out-of-plane polarization and topological magnetic vortices in multiferroic $CrPSe_3$, Phys. Rev. Mater. **6**, L101402 (2022).
[9] M. J. Pitcher, P. Mandal, M. S. Dyer, J. Alaria, P. Borisov, H. Niu, J. B. Claridge, and M. J. Rosseinsky, Tilt engineering of spontaneous polarization and magnetization above 300 K in a bulk layered perovskite, Science **347**, 420 (2015).
[10] L. D. Landau, L. Pitaevskii, A. M. Kosevich, and E. M. Lifshitz, *Theory of Elasticity: Volume 7* (Elsevier, New York, 2012).
[11] L. D. Landau and E. M. Lifshitz, *Statistical Physics: Volume 5* (Elsevier, New York, 2013).
[12] N. A. Benedek and C. J. Fennie, Hybrid improper ferroelectricity: A mechanism for controllable polarization-magnetization coupling, Phys. Rev. Lett. **106**, 107204 (2011).
[13] J.-J. Zhang, L. Lin, Y. Zhang, M. Wu, B. I. Yakobson, and S. Dong, Type-II multiferroic $Hf_2VC_2F_2$ MXene monolayer with high transition temperature, J. Am. Chem. Soc. **140**, 9768 (2018).
[14] H. Schmid, Some symmetry aspects of ferroics and single phase multiferroics, J. Phys. Condens. Matter **20**, 434201 (2008).
[15] X. Li, C. Xu, B. Liu, X. Li, L. Bellaiche, and H. Xiang, Realistic spin model for multiferroic NiI_2, Phys. Rev. Lett. **131**, 036701 (2023).

[16] C. Liu, W. Ren, and S. Picozzi, Spin-chirality-driven multiferroicity in van der Waals monolayers, Phys. Rev. Lett. **132**, 086802 (2024).
[17] S. Xu, X. Wang, L. Bellaiche, and B. Xu, Electric control of magnetism in multiferroic rare-earth-substituted $BiFeO_3$ with ferrielectricity, Phys. Rev. Lett. **133**, 046801 (2024).
[18] D. Shin, S. Latini, C. Schäfer, S. A. Sato, E. Baldini, U. De Giovannini, H. Hübener, and A. Rubio, Simulating terahertz field-induced ferroelectricity in quantum paraelectric $SrTiO_3$, Phys. Rev. Lett. **129**, 167401 (2022).
[19] W. Eerenstein, N. D. Mathur, and J. F. Scott, Multiferroic and magnetoelectric materials, Nature (London) **442**, 759 (2006).
[20] J. H. Lee *et al.*, A strong ferroelectric ferromagnet created by means of spin-lattice coupling, Nature (London) **466**, 954 (2010).
[21] A. Planes, T. Castan, and A. Saxena, Thermodynamics of multicaloric effects in multiferroics, Philos. Mag. **94**, 1893 (2014).
[22] A. Edström and C. Ederer, Prediction of a giant magnetoelectric cross-caloric effect around a tetracritical point in multiferroic $SrMnO_3$, Phys. Rev. Lett. **124**, 167201 (2020).
[23] D. Khomskii, Classifying multiferroics: Mechanisms and effects, Physics **2**, 20 (2009).
[24] See Supplemental Material at http://link.aps.org/supplemental/10.1103/PhysRevLett.134.216801 for SM1, computational details; SM2, computational details about Berry phase calculations; SM3, energy barrier between ferroelectric and magnetic phases in autferroics; SM4, Ginzburg-Landau theory for MC simulation and design rules for autferroics in real materials; SM5, design rules for autferroics in real materials; SM6, magnetic phase in the $TiGeSe_3$ monolayer; SM7, ferroelectric phase in the $TiGeSe_3$ monolayer; SM8, magnetoelectric coupling in the $TiGeSe_3$ monolayer; and SM9, autferroics under a magnetic field, including Refs. [7,11,25–34].
[25] M. E. Newman and G. T. Barkema, *Monte Carlo Methods in Statistical Physics* (Clarendon Press, Oxford, 1999).
[26] J. D. Alzate-Cardona, D. Sabogal-Suárez, R. F. L. Evans, and E. Restrepo-Parra, Optimal phase space sampling for Monte Carlo simulations of Heisenberg spin systems, J. Phys. Condens. Matter **31**, 095802 (2019).
[27] G. Kresse and J. Furthmüller, Efficient iterative schemes for *ab initio* total-energy calculations using a plane-wave basis set, Phys. Rev. B **54**, 11169 (1996).
[28] G. Kresse and D. Joubert, From ultrasoft pseudopotentials to the projector augmented-wave method, Phys. Rev. B **59**, 1758 (1999).
[29] G. I. Csonka, J. P. Perdew, A. Ruzsinszky, P. H. T. Philipsen, S. Lebègue, J. Paier, O. A. Vydrov, and J. G. Ángyán, Assessing the performance of recent density functionals for bulk solids, Phys. Rev. B **79**, 155107 (2009).
[30] R. D. King-Smith and D. Vanderbilt, Theory of polarization of crystalline solids, Phys. Rev. B **47**, 1651 (1993).
[31] R. Resta, M. Posternak, and A. Baldereschi, Towards a quantum theory of polarization in ferroelectrics: The case of $KNbO_3$, Phys. Rev. Lett. **70**, 1010 (1993).
[32] R. Resta, Macroscopic polarization in crystalline dielectrics: the geometric phase approach, Rev. Mod. Phys. **66**, 899 (1994).
[33] J. B. Goodenough, An interpretation of the magnetic properties of the perovskite-type mixed crystals $La_{1-x}Sr_xCoO_{3-\lambda}$, J. Phys. Chem. Solids **6**, 287 (1958).
[34] J. Kanamori, Superexchange interaction and symmetry properties of electron orbitals, J. Phys. Chem. Solids **10**, 87 (1959).
[35] K. Hayakawa, S. Kanai, T. Funatsu, J. Igarashi, B. Jinnai, W. A. Borders, H. Ohno, and S. Fukami, Nanosecond random telegraph noise in in-plane magnetic tunnel junctions, Phys. Rev. Lett. **126**, 117202 (2021).
[36] H. Jiang, D. Belkin, S. E. Savel'ev, S. Lin, Z. Wang, Y. Li, S. Joshi, R. Midya, C. Li, M. Rao *et al.*, A novel true random number generator based on a stochastic diffusive memristor, Nat. Commun. **8**, 882 (2017).
[37] E. A. Eliseev, M. D. Glinchuk, V. Khist, V. V. Skorokhod, R. Blinc, and A. N. Morozovska, Linear magnetoelectric coupling and ferroelectricity induced by the flexomagnetic effect in ferroics, Phys. Rev. B **84**, 174112 (2011).
[38] E. A. Eliseev, Complete symmetry analyses of the surface-induced piezomagnetic, piezoelectric and linear magnetoelectric effects, Ferroelectrics **417**, 100 (2011).
[39] P. R. Mickel, H. Jeen, P. Kumar, A. Biswas, and A. F. Hebard, Proximate transition temperatures amplify linear magnetoelectric coupling in strain-disordered multiferroic $BiMnO_3$, Phys. Rev. B **93**, 134205 (2016).
[40] P.-W. Ma, S. L. Dudarev, and J. S. Wróbel, Dynamic simulation of structural phase transitions in magnetic iron, Phys. Rev. B **96**, 094418 (2017).

End Matter

EM1: More details of exclusion of bilinear magnetoelectric coupling term in Eq. 1.—The Landau free energy is a scalar, which should be time-reversal invariant and space-inversion invariant. As a result, a bilinear magnetoelectric coupling term $\mathbf{M}\cdot\mathbf{P}$ (or $\mathbf{M}\times\mathbf{P}$) is generally not allowed as symmetry violating. Although in some cases with special magnetic point groups, the bilinear magnetoelectric term seems to be allowed [37,38], the fact is that their coefficients of bilinear magnetoelectric term are not regular scalars but vectors or tensors, which break both the time-reversal and space-inversion symmetries. Then the physical information of magnetism/space is already hidden in such coefficients. For example, the magnetoelectric term can be like $\mathbf{L}\cdot(\mathbf{M}\times\mathbf{P})$ [39], where the staggered order parameter L representing an antiferromagnetic background is used to preserve inversion and time-reversal symmetry. Then if one assumes invariant L, it can be simplified as $(M\times P)$ nominally, although in fact here M is not a primary order parameter anymore. In a

primary study here, our form of Landau free energy is intended for the most generic cases, with M and P as order parameters and scalar coefficients.

EM2: Difference between multiferroics and autferroics—In the multiferroic systems [19–22], ferroelectricity and magnetism coexist within the same material due to their attractive or weakly repulsive biquadratic magnetoelectric coupling. In contrast, in the present case (autferroics), the strongly repulsive biquadratic magnetoelectric coupling eliminates the coexistence of ferroelectricity and magnetism. Thus, autferroics represent a unique material family and can be regarded as a sister branch of the multiferroic family. As clearly illustrated in Fig. 1(a), the autferroic region is isolated from the multiferroic region by the middle single-ferroic one.

EM3: Difference between single-ferroics and autferroics—Generally, Eq. 1 exhibits four solutions [22], i.e, nonferroic ($P=0$, $M=0$), magnetic ($P=0$, $M\neq 0$), ferroelectric ($P\neq 0$, $M=0$), and multiferroic ($P\neq 0$, $M\neq 0$). However, it should be noted that only ($P=0$, $M\neq 0$) or ($P\neq 0$, $M=0$) is not enough to define autferroics. For example, in the single-ferroic region [i.e., the middle region between multiferroic and autferroic of Fig. 1(a)], these two solutions can exist: one as the ground state and another as an energetic saddle point, as shown in Fig. 1(c). However, ($P\neq 0$, $M=0$) and ($P=0$, $M\neq 0$) solutions in autferroics are (meta)stable with isolated energy wells for each state and energy barriers between them [Fig. 1(d)]. Without these energy wells and energy barriers, ($P\neq 0$, $M=0$) and ($P=0$, $M\neq 0$) can only be considered as single-ferroics at most, instead of autferroics. A key physical difference between the single-ferroic and autferroic solutions is the magnetoelectric response. For example, an electric field can switch the phase of autferroics between the ferroelectric state and magnetic state [24], while for the single-ferroic one the switching can only be done between $+P$ and $-P$.

EM4: Ginzburg-Landau theory for MC simulation—Although the Heisenberg model can deal with the magnetic transition in multiferroics, this model cannot deal with the phase transition in autferroics. The most important property in autferroicity is the switching between ferroelectricity and magnetism. Hence, we used the standard Landau-type free energy terms for magnetism. Here, the Ginzburg-Landau theory is used in our MC simulation.

Then Eq. 1 is turned into two individual lattice sites as follows [11]:

$$F=\sum_i\left(-aP_i^2+bP_i^4\right)+\sum_{\langle i,j\rangle}\upsilon_P(P_i-P_j)^2+\sum_k\left(-dM_k^2+eM_k^4\right)+\sum_{\langle k,l\rangle}\upsilon_M(M_k-M_l)^2+\sum_{\langle i,k\rangle}cP_i^2M_k^2. \tag{D1}$$

Here, the local site magnetic energy and polar energy (the 1st and 3rd terms in Eq. D1, respectively) are the standard Landau-type free energy terms (Eq. 1), which leads to independent magnetization (M_s or $-M_s$) and polarization (P_s or $-P_s$). Similar to the Heisenberg model, directional shifts of spin at neighboring sites induce energy fluctuations (the 2nd term), described by the Ginzburg term, i.e., $\upsilon_M(\nabla M)^2$. The coefficient υ_M represents the magnetic stiffness (similar to the nearest-neighbor magnetic coupling J in the Heisenberg model [24]). As a beginning model for autferroicity, here the order parameters (M and P) are simplified as scalars, as done in standard mean field approximation.

EM5: Form of magnetoelectric coupling in autferrocity—Taking the $TiGeSe_3$ monolayer as a typical example, ferroelectricity and magnetism originate from Ge-Ge and Ti honeycomb lattices, respectively. Therefore, in our MC simulation, we adopted two sublattices (ferroelectric triangle + magnetic honeycomb) with the nested geometry as in $TiGeSe_3$. Thus, for each Ti site, it has three ferroelectric neighboring sites, as shown in Fig. 5. The biquadratic magnetoelectric coupling term in Eq. D1 quantitatively accounts for the mutual exclusivity between these ferroelectric and magnetic lattices. Here the magnetoelectric interactions are represented by the coupling term between these two sublattices, expressed as $P_i^2M_k^2$, which is summed over nearest-neighbors between ferroelectric sites i and magnetic site k [Fig. 5(a) inset]. Obviously, this coupling term in autferroics does

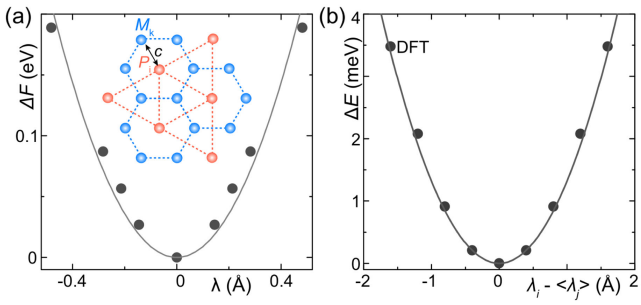

FIG. 5. (a) Fitting of ME coefficient in $TiGeSe_3$. ΔF as a function of λ in the S-AFM state. Inset: illustration of the magnetoelectric interaction between the ferroelectric P_i lattice and the magnetic M_k lattice as used in Eq. D1. (b) Fitting of dipole-dipole interaction in the $TiGeSe_3$ monolayer using the mean field theory, i.e., the coefficient υ_P. The black points are the DFT-calculated energy of different displacements $\lambda_i-\langle\lambda_j\rangle$.

not describe on site interactions but rather interactions between the ferroelectric and magnetic lattices.

EM6: Extracting the Landau parameters from DFT calculations—(a) $T = 0$ K case. The Ginzburg terms in Eq. D1 are absent ($\nabla M = 0$ and $\nabla P = 0$). Using the pure ferroelectric phase (nonmagnetic phase, $M = 0$), the ferroelectric Landau parameters a and b ($\tilde{a}$ and $\tilde{b}$) are obtained by fitting the ferroelectric double-well potential [Fig. 3(b)], which is obtained from DFT calculations. Similarly, the magnetic Landau parameters d and e are extracted from a pure magnetic phase ($P = 0$). Unlike ferroelectric polarization, the single atom's magnitude of magnetic moment cannot continuously vary from 0 to M_s. Here, taking the high symmetry phase ($P = 0$, $M = 0$) as a reference, the energy difference between the ($P = 0$, $M = 0$) and ($P = 0$, $M = M_s$) phases can be calculated in the DFT. We can identify the energy difference per magnetic atom $\Delta E_M = -dM_s^2 + eM_s^4$ and the magnitude of magnetic moment $M_s = \sqrt{d/2e}$. Hence, the values of d and e are calculated by solving these equations [40].

(b) $T \neq 0$ K case. At the finite temperature, the Ginzburg terms, i.e., $\upsilon_M(\nabla M)^2$ for magnetism and $\upsilon_P(\nabla P)^2$ for ferroelectricity, are included in Eq. D1 to account for thermal fluctuations. It is important to note that Ginzburg terms only affect the transition temperature, such as the transition from an autferroic to a single-ferroic phase. In MC simulations, the coefficient υ_M in Eq. D1 is calculated via DFT calculations of various pure magnetic structures, e.g., ferromagnetic and different antiferromagnetic phases, following a similar approach to calculating the magnetic coupling coefficient J in the Heisenberg model. In the $TiGeSe_3$ monolayer, for pure magnetic transition, the Ginzburg-Landau theory leads to similar T_C to that obtained using the Heisenberg model [Figs. S4(a) and S2(b)]. For ferroelectric υ_P coefficient, we calculated energy difference (ΔE) as a function of $P_i - \langle P_j \rangle$ (or $\lambda_i - \langle \lambda_j \rangle$) using DFT within the standard mean field approximation, which follows a quadratic relationship [Fig. 5(b) for the $TiGeSe_3$ monolayer with ferroelectric activity (Ti^{4+} state)]. The coefficient υ_P is then obtained by fitting the quadratic term.